Optical Engineering

OpticalEngineering.SPIEDigitalLibrary.org

Measurement of initial displacement of canine and molar in human maxilla under different canine retraction methods using digital holographic interferometry

Manoj Kumar
Anshu Singh Birhman
Sridhar Kannan
Chandra Shakher

Manoj Kumar, Anshu Singh Birhman, Sridhar Kannan, Chandra Shakher, "Measurement of initial displacement of canine and molar in human maxilla under different canine retraction methods using digital holographic interferometry," *Opt. Eng.* **57**(9), 094106 (2018), doi: 10.1117/1.OE.57.9.094106.

Measurement of initial displacement of canine and molar in human maxilla under different canine retraction methods using digital holographic interferometry

Manoj Kumar,[a] Anshu Singh Birhman,[b] Sridhar Kannan,[b] and Chandra Shakher[a,*]
[a]Indian Institute of Technology Delhi, Laser Applications and Holography Laboratory, Instrument Design Development Centre, Hauz Khas, New Delhi, India
[b]Manav Rachna Dental College, Department of Orthodontics and Dentofacial Orthopedics, Faridabad, Haryana, India

Abstract. An application of digital holographic interferometry for the measurement of the initial displacement of canine and molar in the human maxilla, under different canine retraction mechanisms, is presented. The objective of this study is to determine and compare the canine and molar displacements with and without transpalatal arch (TPA) on 0.018-in. stainless steel (SS) and 0.019- × 0.025-in. SS arch-wires, using three different canine retraction sliding mechanism methods: nickel–titanium (Ni–Ti)-closed coil-spring, active tie-back, and elastomeric chains. The proposed technique is highly sensitive and enables the displacement measurement of the canine and molar in human maxilla under different canine retraction methods, more precisely and accurately compared with its counterparts. The experiment was conducted on a dry human skull without mandible with intact dental arches and aligned teeth. The experimental results reveal that Ni–Ti-closed coil-spring produces maximum initial canine displacement, followed by active-tie back and elastomeric chain. It was also found that initial canine and molar displacements were more on 0.018-in. SS arch-wire as compared with 0.019 × 0.025-in. SS arch-wire. Further, the initial displacement of the molar was less when TPA was taken as an anchorage in comparison to without anchorage. [DOI: 10.1117/1.OE.57.9.094106]

Keywords: digital holographic interferometry; displacement measurement; human maxilla; canine retraction mechanism.

Paper 180817 received Jun. 7, 2018; accepted for publication Aug. 30, 2018; published online Sep. 24, 2018.

1 Introduction

Orthodontic treatment often requires canine retraction and many canine retraction appliances have been used.[1–5] The most common mechanism for making retraction space available involves the extraction of the first premolar in each quadrant. In retracting the anterior, the most common approach is a sequential procedure in which the canines and incisors are retracted in two separate steps. In the first step, the canine in each quadrant is retracted to full contact with the tooth distal to the extraction space. In the second step, the canines are consolidated with the posterior anchorage unit. The resulting grouping is then used as a single anchorage unit to retract the incisors. This procedure has been called the "two-step" technique. The alternative approach is "en-masse retraction" in which the incisors and canines are retracted as a single unit. The two-step technique reduces the tendency of the maxillary molars to displace forward.[6] One of the reliable mechanics used for canine retraction is sliding mechanics.[7] The merits of this mechanism have been reported by Ziegler and Ingervall[8] and Rhee et al.[9]

In the present study, the sliding mechanism has been implemented on 0.018-in. stainless steel (SS) arch-wire and 0.019 × 0.025-in. SS arch-wire with molar as the anchorage unit. The purpose of the study is to measure the initial displacement of the canine and molar on these two arch-wires, under the influence of external force by three different sliding mechanisms of canine retraction methods using a laser-based nondestructive technique. For many decades, the laser-based nondestructive techniques have been utilized in many scientific, engineering, and industrial measurements.[10,11] In the present study, digital holographic interferometry (DHI) has been used for the measurement of the initial displacement of the canine and molar because of its several advantages contrary to conventional holographic interferometry[12] and digital speckle pattern interferometry.[13] This application of DHI could be proven a measurement technique in dentistry because the measurement of deformations/displacements/strain in dentistry is accomplished by the conventional methods such as strain gage or finite-element method (FEM). Without correct boundary conditions, FEM may give wrong results. Moreover, in FEM, the model has to be validated by some other alternative and accurate technique that gives assurance that the results are reasonably accurate/valid. On the other hand, DHI could have the potential for such studies offering several advantages such as this technique is the noncontact type, provides full-field information noninvasively, and more accurate, precise, and robust compared with conventional methods. In this study, three different canine retraction sliding mechanisms were employed with and without transpalatal arch (TPA). These sliding mechanisms are (1) Ni–Ti-closed coil-spring, (2) active tie-back, and (3) elastomeric chains. The experiment was repeated for different force levels (150 and 200 g) of these three-loaded sliding mechanisms in identical conditions to validate the proposed method.

*Address all correspondence to: Chandra Shakher, E-mail: cshakher@iddc.iit.ac.in

0091-3286/2018/$25.00 © 2018 SPIE

Fig. 1 Photographs of the human maxilla with intact dental arches and aligned teeth.

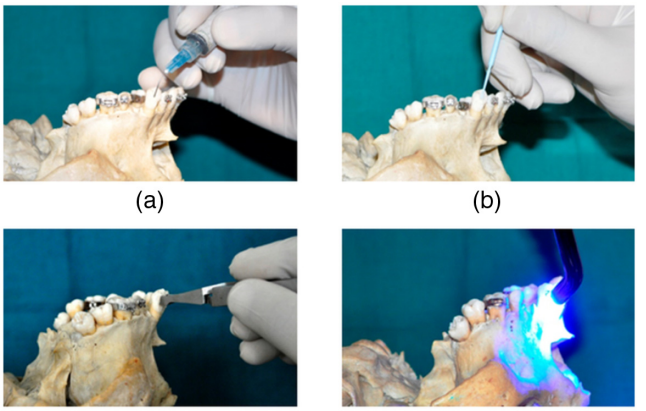

Fig. 2 Photographs showing bonding steps: (a) etching, (b) primer application, (c) bracket placement, and (d) curing.

2 Material

This section presents a brief description of the material and the armamentarium used in the experiment. The experiment was conducted on a dry human skull without mandible with intact and well-aligned maxillary arch as shown in Fig. 1. The skull was mounted on type II dental plaster base that has a bigrooved rectangular base to form a three-dimensional (3-D) stable assembly. The hardness of the skull is 280 BHN (Brinell hardness number), Young's modulus is 13,800 MPa, and Poisson's ratio is 0.26. For the individual canine retraction, the first premolars were extracted bilaterally to create space between the second premolar and canine. As a dry skull becomes brittle and the periodontal space dries out, a vacant space was created between the tooth and bone socket, which causes increase in the tooth movement. To mimic the function of the periodontal ligament in a dry skull, the periodontal space was filled with a layer of Araldite 208 with hardener 596 in the ratio of 1:1, which possesses nearly same elasticity as the periodontal ligament.

Maxillary arch was bonded with the preadjusted appliance, namely McLaughlin Bennett and Trevisi with 0.022- × 0.028-in. slot. Teeth were cleaned and etched with 37% phosphoric acid for 30 s.. Then, the primer was applied on the etched surface and the brackets were placed according to the bonding chart. A curing was done with a LED curing gun to cure the transbond and attach the brackets to the tooth surface. The photographs of these four procedures are shown in Figs. 2(a)–2(d).

The canine retraction was carried out on two arch-wires, namely 0.018-in. SS arch-wire and 0.019- × 0.025-in. SS arch-wire, using Ni–Ti-closed coil spring, active tie-back, and elastomeric chain as sliding mechanisms. Figures 3(a)–3(c) show the photographs of the elastomeric chain, active tie-back, and Ni–Ti-closed coil spring, respectively. The loading of these sliding mechanisms was done with two force levels, such as 150 and 200 g, respectively. The force level was measured with the help of a dynamometer gage (Captain Ortho, Libral Traders Pvt., Ltd., India). Figures 3(d)–3(f) show the photographs of the human maxilla employed with three sliding mechanisms. The anchorage was taken from maxillary first molar with and without TPA as shown in Figs. 3(g) and 3(h), respectively.

3 Theory

Holographic interferometry (HI) was developed by Powell and Stetson[14] and Haines and Hildebrand[15] in late 1960. The use of digital computers and recording devices (CCD/CMOS) led to the development of DHI.[14] The use of digital techniques overcame the problems associated with the conventional holography and made it a more versatile tool for metrology.[16–25] In digital holography, the CCD/CMOS detectors enabled the direct recording of holograms in a digital form. The reconstruction process is then performed numerically.[16–22] Different numerical methods are used for the reconstruction of digital holograms, such as Fresnel,[16,17] lensless Fourier transform (LLFT),[18] convolution,[21] and angular spectrum[22] approaches. The process of numerical reconstruction of complex object wavefront from the recorded digital hologram can be used for the quantitative analysis of the amplitude and the phase of the recorded wavefront. In DHI, the reference wave and the wave scattered from or transmitted from the object are interfered at the faceplate of the CCD/CMOS device. The interference pattern is sampled and digitized by an analog-to-digital (A/D) converter and stored in the memory of a computer. From the recorded digital hologram, the real and virtual object waves can be reconstructed if the diffraction of the reference wave is carried out by numerical methods.[16–22] In this work, LLFT configuration of digital holography is used[23,24] due to its several advantages discussed in Refs. 23 and 24, respectively. In LLFTDHI, the object and point sources of the spherical reference wave are kept in the same plane. The diffraction of reference wave at the hologram can be calculated by Fresnel Kirchhoff integral.[15–17]

Two digital holograms corresponding to two different states of the object are recorded. The first digital hologram was recorded in preloading of the retraction mechanism and another in postloading. The phase distribution of the object wavefronts in two different states of the object is numerically reconstructed by employing Fourier transform method (described in detail in Refs. 23 and 24) separately from the recorded digital holograms. The interference phase, i.e., the phase difference between two states of the object, is calculated directly by modulo 2π subtraction as:[23,24]

$$\Delta\phi(x,y) = \begin{cases} \phi_2(x,y) - \phi_1(x,y); & \text{if } \phi_2(x,y) \geq \phi_1(x,y) \\ \phi_2(x,y) - \phi_1(x,y) + 2\pi; & \text{if } \phi_2(x,y) < \phi_1(x,y) \end{cases}, \tag{1}$$

where $\phi_1(x,y)$ and $\phi_2(x,y)$ are the phase distributions of the object wavefronts in two different states of the object.

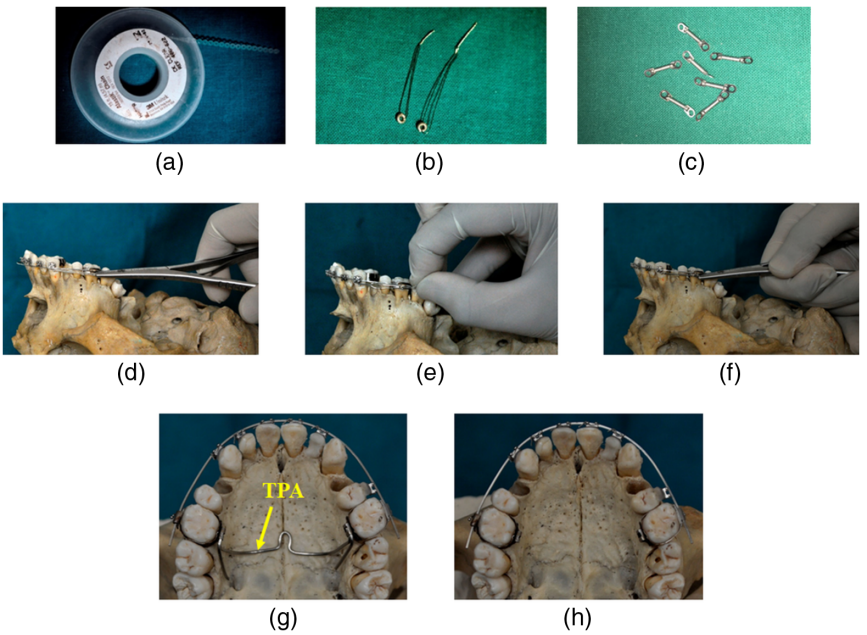

Fig. 3 Photographs of: (a) elastomeric chain, (b) active tie-back, (c) Ni–Ti-closed coil springs, (d) human maxilla with elastomeric chain, (e) human maxilla with active tie-back, and (f) human maxilla with Ni–Ti-closed coil spring, (g) human maxilla with TPA, and (h) human maxilla without TPA.

The calculated interference phase values according to Eq. (1) remain wrapped in the range $(-\pi, +\pi)$ radian, corresponding to the principal value of the arctan function. The numerically calculated interference phase is continuous between 0 and 2π. This 2π phase discontinuity was removed by Goldstein phase unwrapping method[26] that consists of adding and subtracting suitable integer multiples of 2π phase values at all points. In DHI, the accurate quantitative continuous

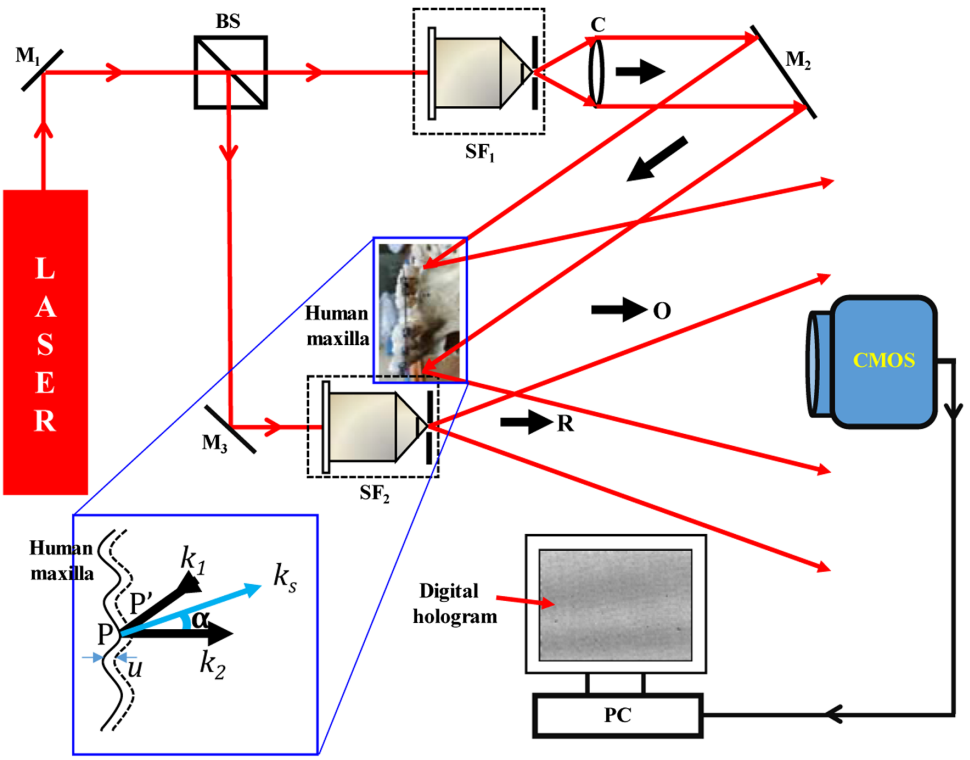

Fig. 4 Schematic of the experimental setup used for the recording of digital holograms.[23] The inset diagram shows the geometric relations between the illumination (k_1), the observation vectors (k_2), and the sensitivity vector (k_s).

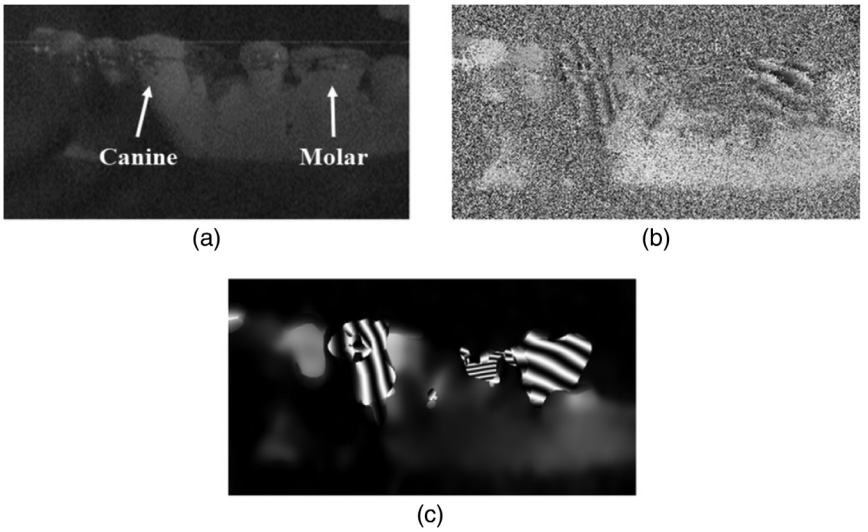

Fig. 5 (a) Reconstructed image of the human maxilla, (b) reconstructed wrapped phase difference map of the canine and molar corresponding to two different holograms recorded at pre- and postloading of the elastomeric retraction spring, and (c) filtered wrapped phase difference map corresponding to Fig. 5(b).

unwrapped phase is directly connected to the change in the state of the object. The deformation, $u(x, y)$, due to the application of load is calculated from the unwrapped phase difference $\Delta\phi(x, y)$ and is given as[25]

$$u(x, y) = \frac{\lambda}{4\pi \cos(\alpha/2)} \Delta\phi(x, y), \tag{2}$$

where α is the angle between the illumination and the observation directions.

4 Experimental Setup

The schematic of the experimental setup used for the measurement of displacements in the molar and canine of human maxilla under different retraction methods using DHI is shown in Fig. 4. During the experiment, a 30-mW He–Ne laser (make—Spectra-Physics, $\lambda = 632.8$ nm) is used as a light source for illumination. The light from the laser is divided into two beams using a beam splitter: one beam is used as the object beam and the second beam is used as a reference beam. The object beam is expanded and filtered using a spatial filter assembly (SF_1) and collimated using a collimator (C). The collimated light is reflected by a mirror (M_2) that illuminates the surface of the object (i.e., human maxilla) under study. The reference beam is also spatially filtered using another spatial filter assembly (SF_2) and brought to focus sideways in the plane of the object. The interference pattern formed by the superposition of the object beam and the reference beam was recorded by the CMOS camera (model—Balser acA2000-340 km) placed at a distance of 95 cm from the object/reference wave plane. The pixel size on the CMOS camera is 5.5 μm × 5.5 μm and the total numbers of pixels are 2048 × 1088 pixels with sensor chip dimension of 11.26 mm × 5.98 mm, respectively. The computer used in this experiment has a 32-bit Intel Pentium IV microprocessor with a CPU clock rate of 3.4 GHz.

The scattered light, O, from the human maxilla interferes with the spatially filtered reference beam, R. The interference pattern formed between object and reference beams is

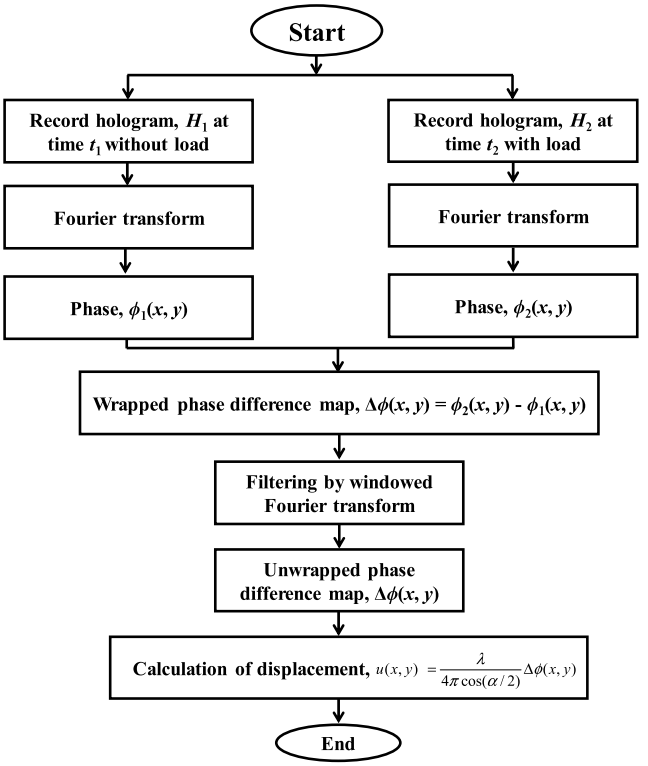

Fig. 6 Flowchart of the experiment and process for calculation of the displacement in canine/molar in human maxilla using DHI. One hologram, H_1, is recorded before and a second hologram, H_2, after the deformation. Fourier transform is employed to retrieve the object's phase and intensity distributions. The intensity distribution is shown in Fig. 5(a). The phase distributions (ϕ_1 and ϕ_2) of the object wavefronts from the two different digital holograms corresponding to two different states are evaluated separately and subtracted to obtain the interference phase difference ($\Delta\phi$) as shown in Fig. 5(b). This wrapped phase difference is filtered by WFT and unwrapped using Goldstein phase unwrapping method. Finally, the displacement in the canine/molar is calculated from this unwrapped phase difference map using Eq. (2).

recorded and stored in the computer and treated as a reference digital hologram. Now the load is applied in the form of a retraction springs (either of Ni–Ti-closed coil-spring, active tie-back, or elastomeric chains), and a digital hologram, due to phase changes, was recorded. The image is reconstructed numerically by employing Fourier transform method. Figure 5(a) shows the numerically reconstructed image of the human maxilla. The image processing was carried out in the MATLAB (version 7.9.0) environment. The wrapped phase difference between the two recorded digital holograms corresponding to two different states of the object (pre- and postloading states) is observed by subtracting the phases of individually reconstructed images. Figure 5(b) shows the reconstructed wrapped phase difference map of the canine and molar corresponding to two different holograms recorded at pre- and postloading of the elastomeric retraction spring with a force level of 150 g.

4.1 *Filtering Scheme Implemented on Noisy Wrapped Phase Difference Map*

The obtained wrapped phase difference map is shown in Fig. 5(b), which contains inherent speckle noise that requires a filtering technique to minimize the speckle noise, enhance the signal-to-noise (SNR), in the wrapped phase difference map, and obtain accurate quantitative information. Speckle noise in the reconstructed image is generated due to the coherent imaging and signal discretization process. The presence of speckle noise may disturb the efficiency and the precision of the phase unwrapping. Different methodologies, such as median, Lee, Kaun, Frost, Gamma, and geometric filtering wavelet filtering, and windowed Fourier filtering (WFF)[27–37] can be implemented to reduce the speckle noise in the reconstructed image from digital holograms, depending upon the measurement applications, such as deformation, measurement of strain, dynamic strain, and

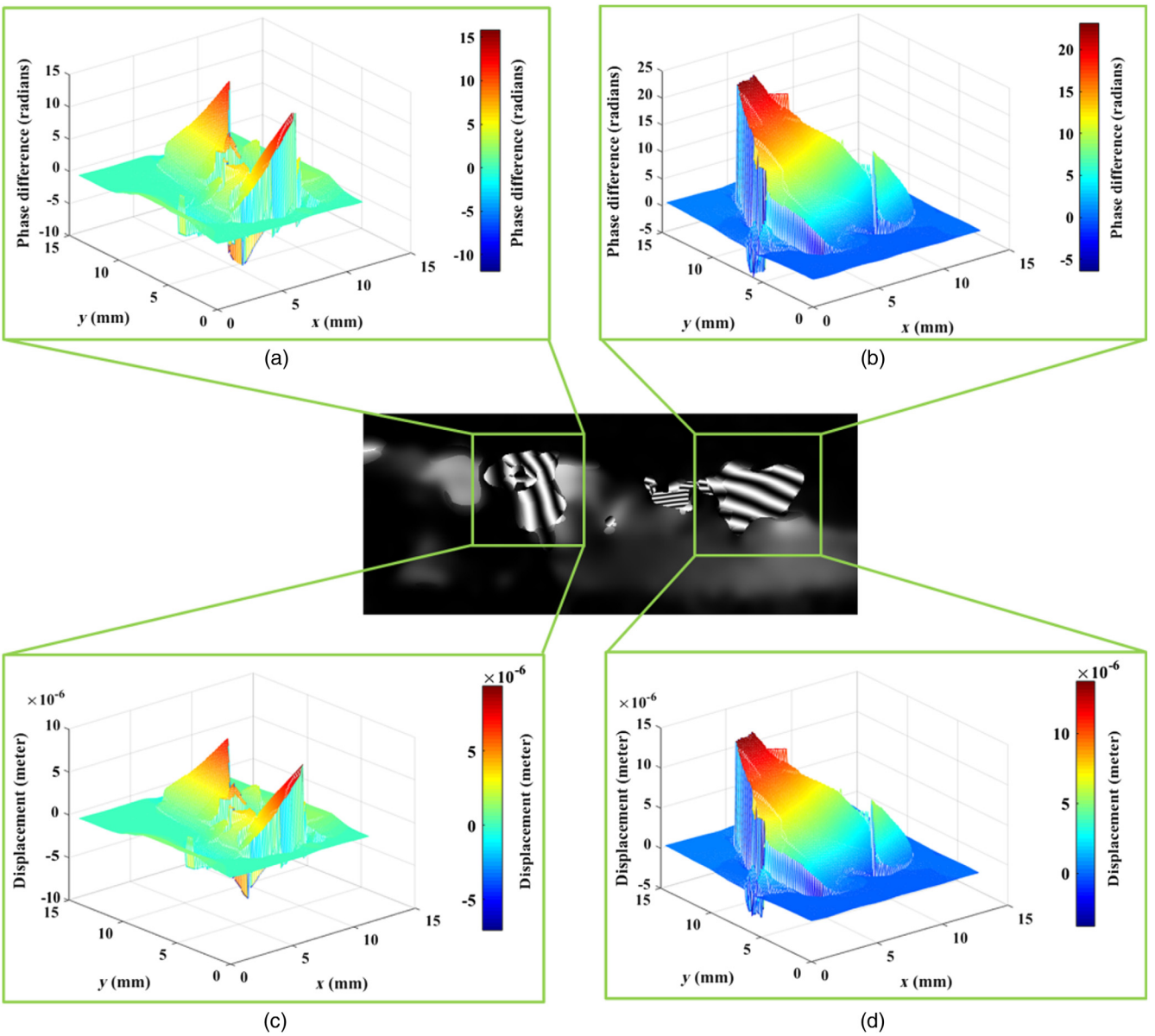

Fig. 7 Unwrapped phase difference map of the (a) canine and (b) molar; 3-D displacement map of the (c) canine and (d) molar.

contouring. In the present case, we implemented WFF[36,37] scheme to the noisy phase map to reduce the speckle noise and to enhance the SNR before phase unwrapping. In WFF, a noisy fringe is transformed by a windowed Fourier transform (WFT) operation into its spectrum. The noise is spread throughout the whole spectrum domain with a small coefficient because of its randomness and incoherence. The noise can be suppressed by discarding the spectrum coefficient if their amplitudes are smaller than a present threshold. The inverse WFT is implemented to produce the smother image.[36] Figure 5(c) shows the filtered wrapped phase difference map corresponding to Fig. 5(b). Figure 6 shows flowchart of executing the experiment and the process of calculating the displacement in the canine and molar of the human maxilla.

Table 1 Maximum initial displacement (in μm) of the molar and the canine on 0.018-in. SS arch-wires (circular in shape) and 0.019- $\times$ 0.025-in. SS arch-wires (rectangular in shape), in human maxilla under different retraction springs without and with TPA.

Wire	With/ without TPA	Retraction spring	Force level (gm)	Displacement (μm) of	
				Molar	Canine
0.018-in. SS arch-wires (circular in shape)	Without TPA	Active tieback	150	10.15	6.10
			200	12.85	7.76
		Elastomeric chain	150	13.89	9.01
			200	17.75	11.19
		Spring coil	150	11.13	10.5
			200	17.66	13.01
	With TPA	Active tieback	150	7.21	10.36
			200	8.69	12.18
		Elastomeric chain	150	7.75	11.60
			200	9.56	13.93
		Spring coil	150	7.81	12.22
			200	8.44	14.02
0.019 $\times$ 0.025-in. SS arch-wires (rectangular in shape)	Without TPA	Active tieback	150	8.86	5.41
			200	11.07	6.63
		Elastomeric chain	150	12.09	7.90
			200	16.15	10.03
		Spring coil	150	9.74	9.29
			200	16.12	11.83
	With TPA	Active tieback	150	6.19	8.98
			200	7.33	11.00
		Elastomeric chain	150	6.40	10.26
			200	8.60	12.53
		Spring coil	150	6.59	11.06
			200	7.19	12.48

5 Results

The calculated phase difference map, as shown in Fig. 5(c), is continuous between 0 and 2π. The 0 to 2π phase discontinuity was removed using the Goldstein phase unwrapping method. Figure 7(a) shows the unwrapped phase difference distribution of the canine and Fig. 7(b) shows the unwrapped phase difference maps of the molar corresponding to Fig. 5(c). The unwrapped phase difference maps give the phase change values that are directly proportional to the displacement. The calculated unwrapped phase difference distribution was used to calculate the displacement of the molar and the canine using Eq. (2). Figures 7(c) and 7(d) show the calculated displacement in the canine and the molar of the human maxilla, respectively, resulting from the loading of elastomeric retraction chain with the force level of 150 g corresponding to the phase difference map shown in Fig. 5(c).

The procedure was repeated to calculate the displacement in molar and canine in human maxilla for three different retraction springs at different force levels (150 and 200 g) with and without TPA. The 3-D displacement plot of the molar and canine for different retraction springs at different force levels with and without TPA is shown in the Appendix. Table 1 shows the measured values of maximum initial displacement in the molar and in the canine on 0.018-in. SS (circular in shape) arch-wires and 0.019- $\times$ 0.025-in. SS (rectangular in shape) arch-wires, for three different retraction springs at different force levels (150 and 200 g) without and with TPA.

Figures 8 and 9 show the comparison of the measured initial displacement of the canine and the molar in human maxilla with and without anchorage using 0.018-in. SS arch-wire for three different sliding mechanisms. A similar comparison between the measured initial displacement of the canine and the molar with and without anchorage using 0.019- $\times$ 0.025-in. SS arch-wire for three different sliding mechanisms is shown in Figs. 10 and 11, respectively.

6 Discussion

The previous studies[38–41] of force–displacement characteristics of teeth have yielded low predictive capability. These studies employed forces that produce a 3-D displacement of the tooth and the tooth displacements were measured by conventional methods. Wedendal and Bjelkhagen[42] and Pryputniewicz[12] developed a holographic interferometric technique that allows noninvasive measurements of tooth displacements. Soon after, other studies[43–46] were investigated in orthodontics by different interferometric techniques. In the present study, a uniform method of canine retraction was performed using three different sliding methods using closed coil spring, active tie back, and elastomeric chain, on a dry human skull with a full maxillary arch-fixed orthodontic metal appliance from right first permanent molar to the left first permanent molar. These canine retraction methods were then attached to the molar for determining the difference in efficacy on two cross-sections of wires 0.018-in. SS and 0.019- $\times$ 0.025-in. SS taking TPA as an anchorage and without anchorage. The initial displacements were calculated and interpreted experimentally. As this study is based

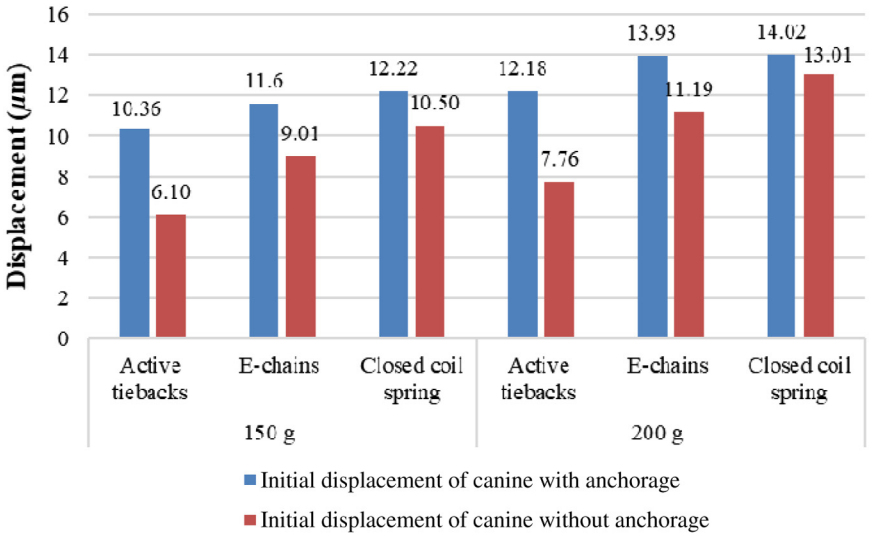

Fig. 8 Initial displacement of the canine with and without anchorage using 0.018-in. SS arch-wire with three different springs at different force levels.

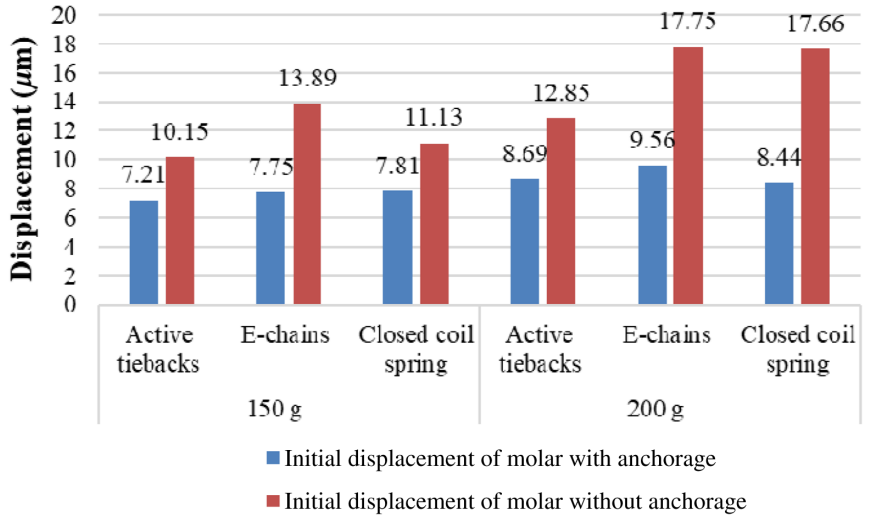

Fig. 9 Initial displacement of the molar with and without anchorage using 0.018-in. SS arch-wire with three different springs at different force levels.

on digital holographic interferometric technique, the results are not based on assumptions that the dental and periodontal structures are geometrically symmetric, homogenous, and isotropic. Therefore, this investigation technique yields more validity to the results as compared with many photoelastic techniques, such as FEM studies, where the anatomy of root, periodontal ligament, and alveolar bone is represented by idealized geometric forms.

Kojima and Fukui[47] conducted an FEM study and concluded that there is no effect of TPA on the initial displacement of anchor tooth, but a mesial tipping is present on the anchor tooth without TPA. However, in this study, the results were showing that there was a slight increase in the initial displacement of molar when TPA was not used. Both arch-wires (i.e., 0.018-in. SS and 0.019- × 0.025-in. SS arch-wires) showed a significant increase in the molar displacement without anchorage as compared with anchorage on different force levels. The initial displacement of canine is increased when TPA was used, as compared to when anchorage was without TPA appliance. When the two molars are reinforced, with TPA appliance offers more resistance to mesial movement of molars and increases the anchorage. Initial displacement, when done on 0.018-in. SS arch-wire and was significantly increased on both 150 and 200 g when compared to without TPA anchorage on both the force levels (i.e., at 150 and 200 g).

According to MBT96, 0.019- × 0.025-in. SS arch-wire is a more suitable wire for canine retraction as compared with 0.018-in. SS arch-wire. This is due to the fact that 0.019 × 0.025-in. SS has less play hence provides less tipping forces on canine and molar. Moreover, 0.018-in. SS arch-wire has also been used widely as it had more play and less frictional forces, more initial displacements, and increased tipping on the canine as well as molar has been observed. In our study,

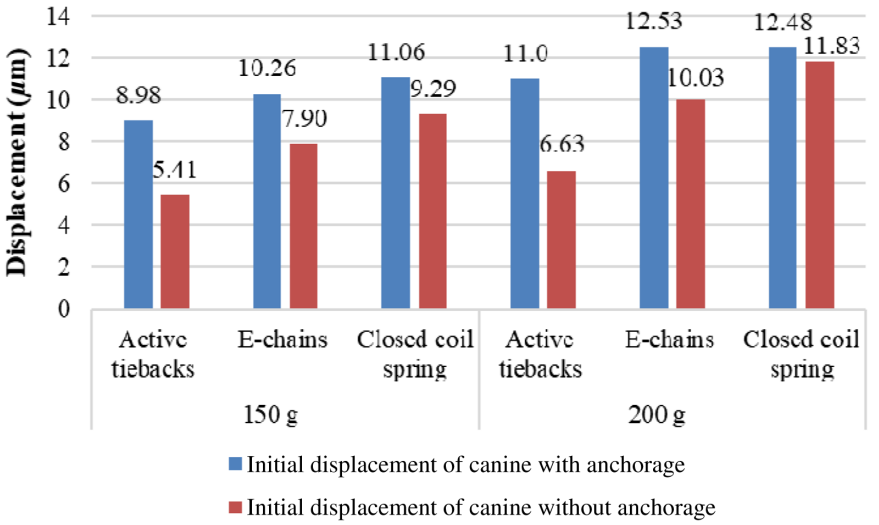

Fig. 10 Initial displacement of the canine with and without anchorage using 0.019- × 0.025-in. SS arch-wire with three different springs at different force levels.

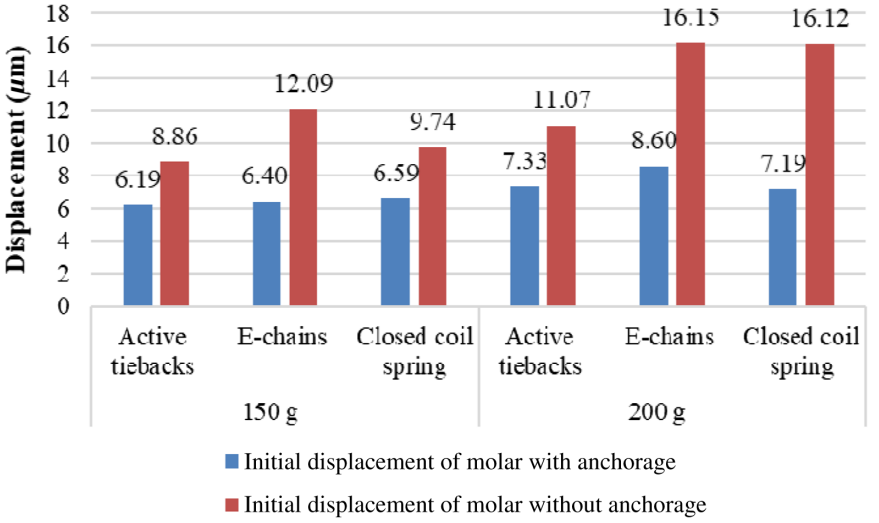

Fig. 11 Initial displacement of the molar with and without anchorage using 0.019- × 0.025-in. SS arch-wire with three different springs at different force levels.

0.018-in. SS arch-wire has shown a significant increase in the initial displacement of canine and molar when compared with 0.019- × 0.025-in. SS arch-wire when all three methods of canine retraction, namely active tie-back, elastomeric chain, and Ni–Ti-closed coil spring, were used.

The measured value of initial displacement of the canine with active tie-back on 150 g of the force level is 10.36 μm on 0.018-in. SS arch-wire, whereas 8.98 μm on 0.019- × 0.025-in.. SS arch-wire; on 200 g of the force level, the displacement value is 12.18 μm on 0.018-in. SS arch-wire, whereas 12.53 μm on 0.019- × 0.025-in. SS arch-wire. Accordingly, initial displacement of the molar with active tie-back on 150 g of the force level is 7.21 μm on 0.018-in. SS arch-wire, whereas 6.19 μm on 0.019- × 0.025-in. SS arch-wire; and on 200 g of force level the displacement value is 8.69 μm on 0.018-in. SS, whereas 7.33 μm on 0.019- × 0.025-in. SS. Similarly, the initial displacement of the canine and the molar with other two sliding mechanisms, with and without TPA, and for different force levels was measured from the obtained phase of difference data.

The comparison between closed coil spring, elastomeric chain, and active tie-back for initial displacement of canine has not been documented before. Closed coil springs that are routinely used for retraction of canine produced maximum canine retraction as compared with other canine retraction methods. Also, the initial displacement of molar, active tie-back produced minimum displacement followed by the closed coil spring and elastomeric chain. Study of initial displacement of teeth gives us an insight into the type of tooth movement that will be finally achieved, as well as stress and strain in the periodontal ligament. The stresses produced in the periodontal ligament when the crown of a tooth is subjected to a force have important ramifications in the study of

orthodontic tooth movement and periodontal research. The noninvasive techniques of laser holography using a dry skull help to find the initial displacement of the teeth.

7 Conclusion

An application of DHI is investigated for the measurement of the initial displacement of the canine and the molar in human maxilla under three different canine retraction sliding mechanisms with and without TPA on 0.018-in. SS and 0.019- × 0.025-in. SS arch-wires. Further, the experiment was repeated for different force levels (150 and 200 g) of the three-loaded sliding mechanisms in identical conditions. The experimentally obtained results reveal that Ni–Ti-closed coil spring produces maximum initial canine displacement, followed by active-tie back and elastomeric chain, respectively. The results show that initial displacements of the canine and molar were more on 0.018-in. SS arch-wire as compared with 0.019 × 0.025-in. SS arch-wire. Further, it was found that the initial displacement of molar was less when TPA was taken as an anchorage in comparison to without anchorage, in all the three sliding canine retraction mechanism methods. The proposed study suggests an appropriate strategy for deformation/displacement/strain measurement in orthodontics.

Appendix: Three-Dimensional Displacement Maps of the Molar and the Canine for Three Different Retraction Springs at Different Force Levels with and Without Transpalatal Arch

Figures 12 and 13 show the displacement map of the molar and canine for the active tie-back chain without TPA and with force levels of 150 and 200 g, respectively.

Similarly, Figs. 14 and 15 show the displacement map of the molar and the canine for the elastomeric chain without TPA and with the force levels of 150 and 200 g, respectively. The displacement map of the molar and the canine for the Ni–Ti-closed spring coil chain without TPA and with the force levels of 150 and 200 g is shown in Figs. 16 and 17, respectively.

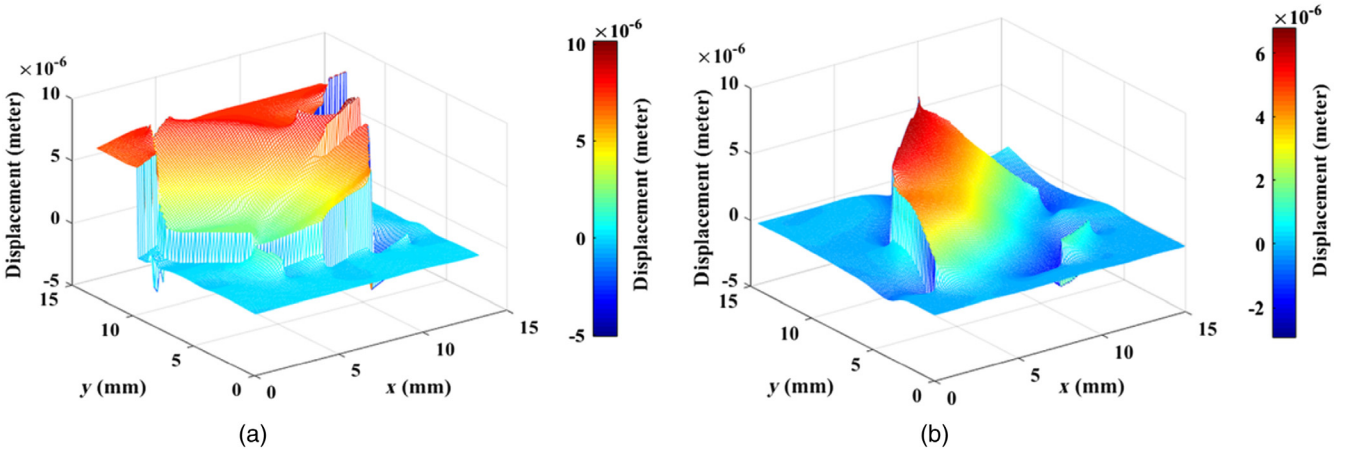

Fig. 12 3-D displacement map of the (a) molar and (b) canine for the active tie-back chain with the force level of 150 g.

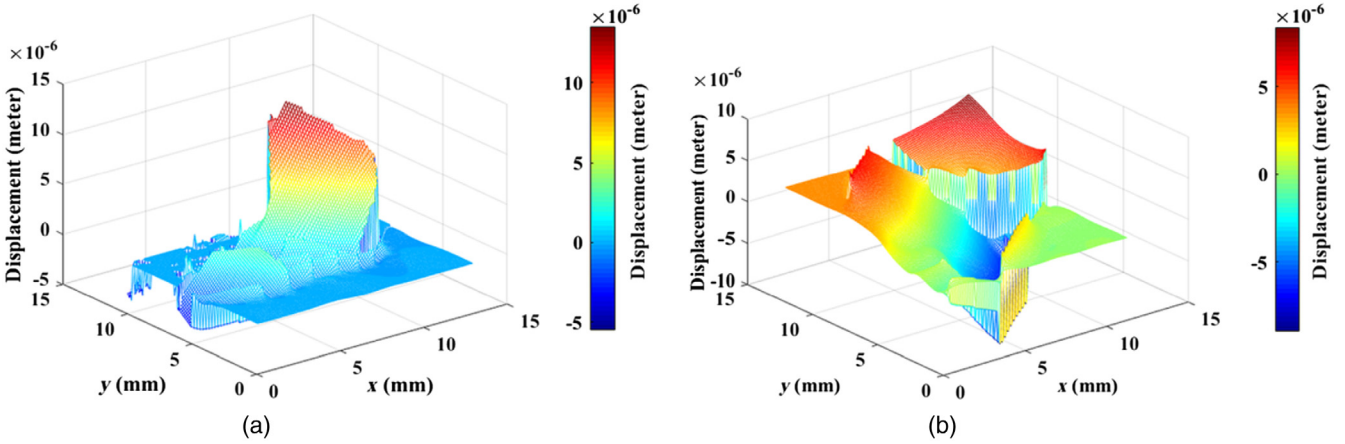

Fig. 13 3-D displacement map of the (a) molar and (b) canine for the active tie-back chain with the force level of 200 g.

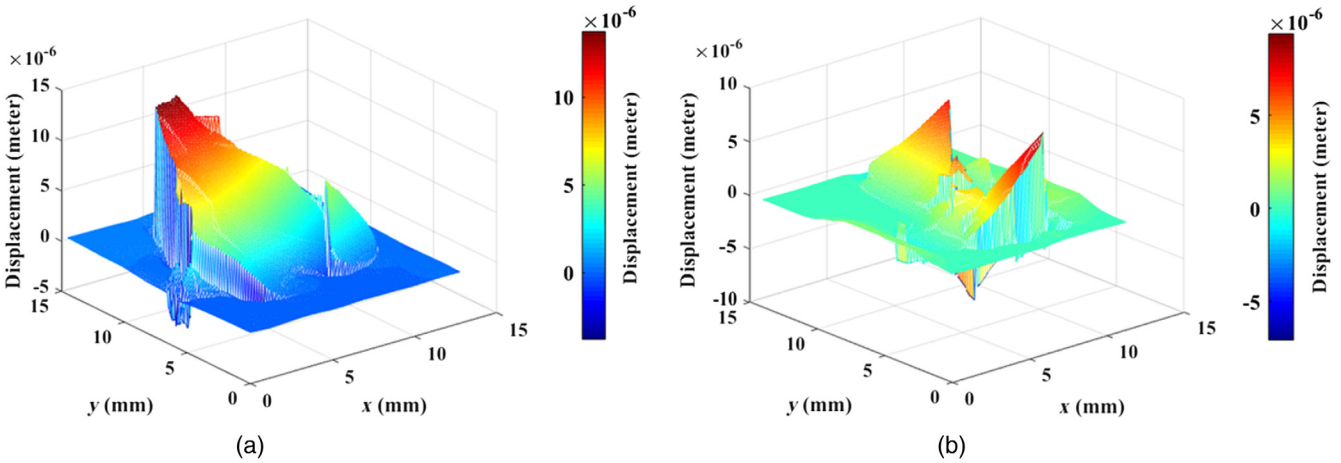

Fig. 14 3-D displacement map of the (a) molar and (b) canine for the elastomeric chain with the force level of 150 g.

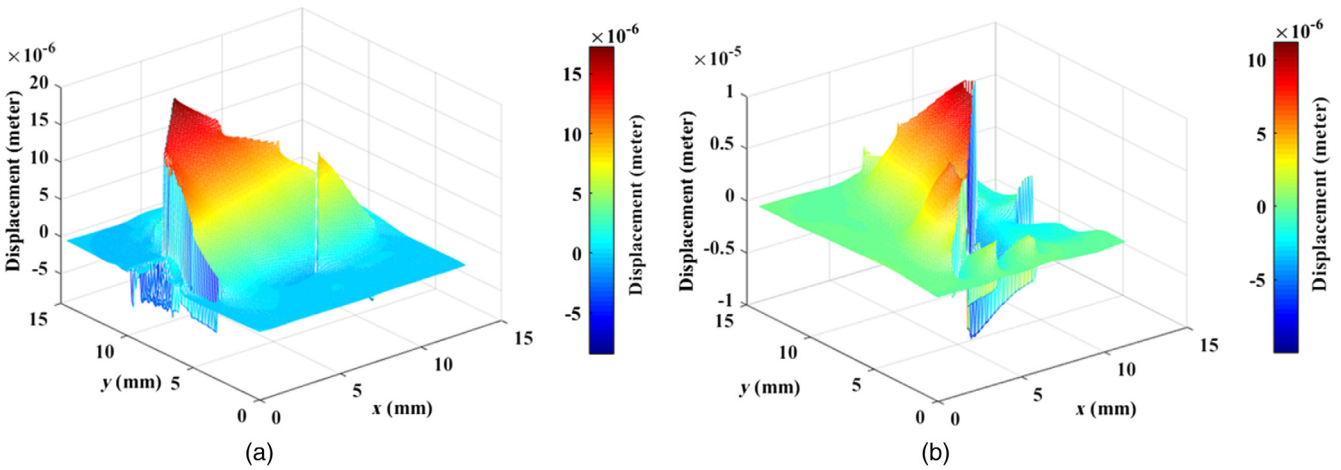

Fig. 15 3-D displacement map of the (a) molar and (b) canine for the elastomeric chain with the force level of 200 g.

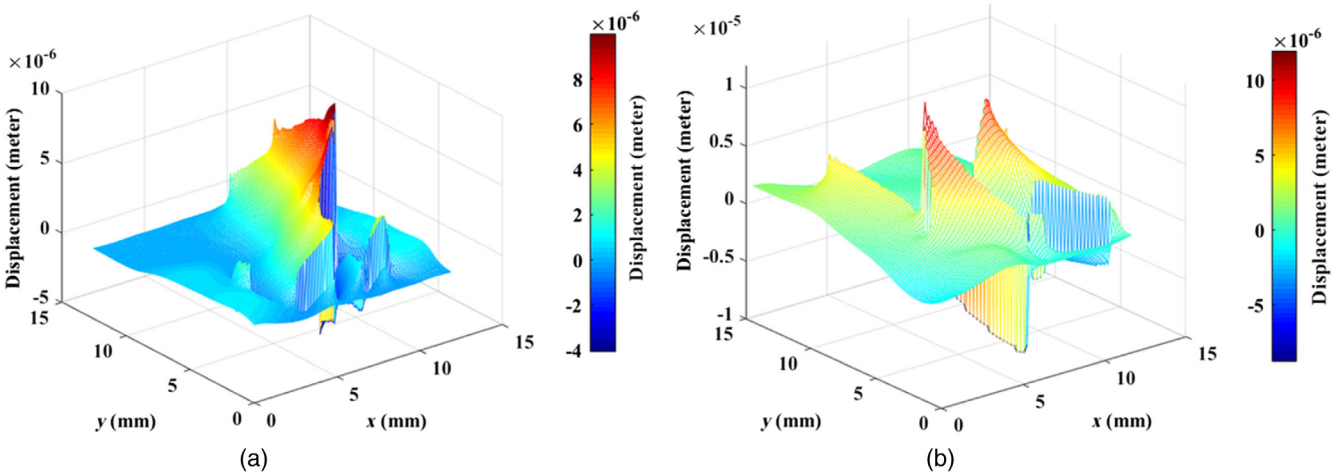

Fig. 16 3-D displacement map of the (a) molar and (b) canine for Ti–Ni-closed coil spring with the force level of 150 g.

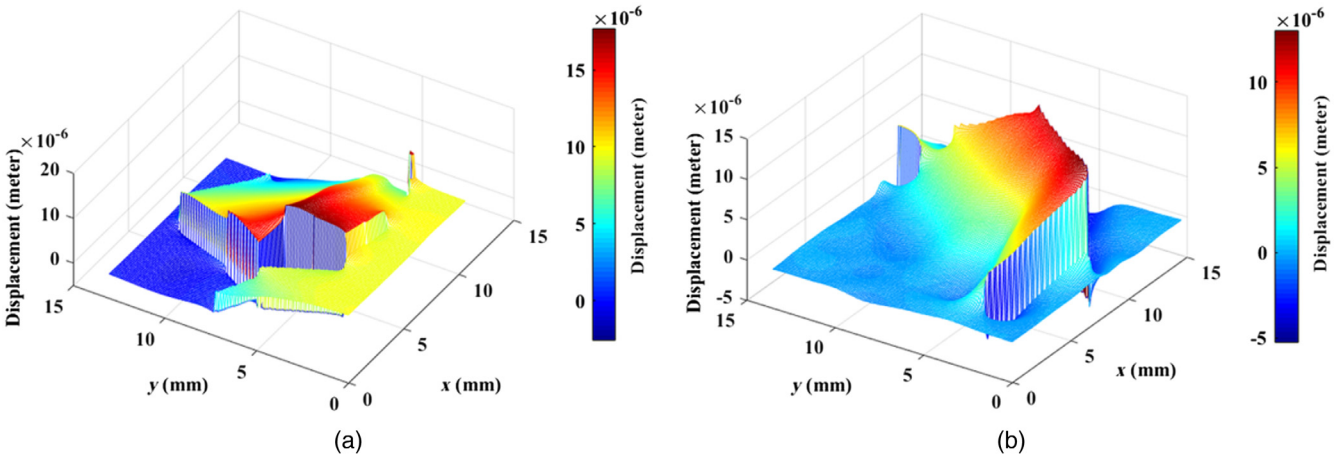

Fig. 17 3-D displacement map of the (a) molar and (b) canine for Ti–Ni-closed coil spring with the force level of 200 g.

Acknowledgments

Dr. Anshu Singh Birhman wishes to thank Dr. Ashish Kumar Singh and Dr. Nitin Arora from Department of Orthodontics and Dentofacial Orthopedics, Manav Rachna Dental College, Faridabad, for their valuable suggestions. The authors gratefully acknowledge the comments and suggestions made by the editor and the reviewers to improve the paper.

References

1. R. M. Ricketts, "Development of retraction sections," *Found. Orthod. Res. Newsl.* **5**, 41–44 (1974).
2. J. C. Burstone, "The segmented arch approach to space closure," *Am. J. Orthod.* **82**, 361–378 (1982).
3. P. Gjessing, "Biomechanical design and clinical evaluation of a new canine-retraction spring," *Am. J. Orthod.* **87**, 353–362 (1985).
4. R. H. A. Samuels et al., "A comparison of the rate of space closure using a nickel–titanium spring and an elastic module: a clinical study," *Am. J. Orthod. Dentofacial Orthop.* **103**, 464–467 (1993).
5. H. Tripolt et al., "Force characteristics of nickel–titanium tension coil springs," *Am. J. Orthod. Dentofacial Orthop.* **115**, 498–507 (1999).
6. R. Sharma et al., "Canine retraction in orthodontics: a review of various methods," *Med. Res. Chron.* **2**, 85–93 (2015).
7. M. S. Block and D. R. Hoffman, "A new device for absolute anchorage for orthodontics," *Am. J. Orthod. Dentofacial Orthop.* **107**, 251–258 (1995).
8. P. Ziegler and B. Ingervall, "A clinical study of maxillary canine retraction with a retraction spring and with sliding mechanics," *Am. J. Orthod. Dentofacial Orthop.* **95**, 99–106 (1989).
9. J.-N. Rhee, Y.-S. Chun, and J. Row, "A comparison between friction and frictionless mechanics with a new typodont simulation system," *Am. J. Orthod. Dentofacial Orthop.* **119**, 292–299 (2001).
10. M. Dekiff et al., "Simultaneous acquisition of 3D shape and deformation by combination of interferometric and correlation-based laser speckle metrology," *Biomed. Opt. Express* **6**, 4825–4840 (2015).
11. I. M. De la Torre et al., "Laser speckle based digital optical methods in structural mechanics: a review," *Opt. Lasers Eng.* **87**, 32–58 (2016).
12. R. J. Pryputniewicz, "Holographic determination of rigid-body motions and application of the method to orthodontics," *Appl. Opt.* **18**, 1442–1444 (1979).
13. M. Kumar et al., "Measurement of strain distribution in cortical bone around miniscrew implants used for orthodontic anchorage using digital speckle pattern interferometry," *Opt. Eng.* **55**, 054101 (2016).
14. R. L. Powell and K. A. Stetson, "Interferometric vibration analysis by wavefront reconstructions," *J. Opt. Soc. Am. A* **55**, 1593–1598 (1965).
15. K. Haines and B. P. Hildebrand, "Contour generation by wavefront reconstruction," *Phys. Lett.* **24**, 422–423 (1965).
16. U. Schnar, "Direct phase determination in hologram interferometry with use of digital recorded holograms," *J. Opt. Soc. Am. A* **11**, 2011–2015 (1994).
17. U. Schnars and W. Jüptner, "Direct recording of holograms by a CCD target and numerical reconstruction," *Appl. Opt.* **33**, 179–181 (1994).
18. C. Wagner et al., "Digital recording and numerical reconstruction of lensless Fourier holograms in optical metrology," *Appl. Opt.* **38**, 4812–4820 (1999).
19. U. Schnars and W. P. O. Juptner, "Digital recording and numerical reconstruction of holograms," *Meas. Sci. Technol.* **13**, R85–R101 (2002).
20. T. M. Kreis, *Handbook of Holographic Interferometry: Optical and Digital Methods*, John Wiley & Sons, Weinheim, Germany (2005).
21. T. M. Kreis, "Frequency analysis of digital holography with reconstruction by convolution," *Opt. Eng.* **41**, 1829–1839 (2002).
22. K. Matsushima, H. Schimmel, and F. Wyrowski, "Fast calculation method for optical diffraction on tilted planes by use of the angular spectrum of plane waves," *J. Opt. Soc. Am. A* **20**, 1755–1762 (2003).
23. M. M. Hossain and C. Shakher, "Temperature measurement in laminar free convective flow using digital holography," *Appl. Opt.* **48**, 1869–1877 (2009).
24. M. Kumar and C. Shakher, "Experimental characterization of the hygroscopic properties of wood during convective drying using digital holographic interferometry," *Appl. Opt.* **55**, 960–968 (2016).
25. D. Dirksena et al., "Lensless Fourier holography for digital holographic interferometry on biological samples," *Opt. Lasers Eng.* **36**, 241–249 (2001).
26. R. M. Goldstein, H. A. Zebker, and C. Werner, "Satellite radar interferometry: two-dimensional phase unwrapping," *Radio Sci.* **23**, 713–720 (1988).
27. J.-S. Lee, "Digital image enhancement and noise filtering by use of local statistics," *IEEE Trans. Pattern Anal. Mach. Intell.* **PAMI-2**, 165–168 (1980).
28. D. T. Kuan et al., "Adaptive noise smoothing filter for images with signal-dependent noise," *IEEE Trans. Pattern Anal. Mach. Intell.* **PAMI-7**, 165–177 (1985).
29. T. R. Crimmins, "Geometric filter for speckle reduction," *Appl. Opt.* **24**, 1438–1443 (1985).
30. A. Lopes et al., "Structure detection and statistical adaptive speckle filtering in SAR images," *Int. J. Remote Sens.* **14**, 1735–1758 (1993).
31. C. Shakher et al., "Application of wavelet filtering for vibration analysis using digital speckle pattern interferometry," *Opt. Eng.* **41**, 176–180 (2002).
32. S. Mirza, R. Kumar, and C. Shakher, "Study of various pre-processing schemes and wavelet filters for speckle noise reduction in digital speckle pattern interferometric fringes," *Opt. Eng.* **44**, 045603 (2005).
33. J. Maycock et al., "Reduction of speckle in digital holography by discrete Fourier filtering," *J. Opt. Soc. Am. A* **24**, 1617–1622 (2007).
34. A. Sharma et al., "Improvement of signal-to-noise ratio in digital holography using wavelet transform," *Opt. Lasers Eng.* **46**, 42–47 (2008).
35. A. Uzan, Y. Rivenson, and A. Stern, "Speckle denoising in digital holography by nonlocal means filtering," *Appl. Opt.* **52**, A195–A200 (2013).
36. Q. Kemao, "Windowed Fourier transform for fringe pattern analysis," *Appl. Opt.* **43**, 2695–2702 (2004).
37. Q. Kemao, "Two-dimensional windowed Fourier transform for fringe pattern analysis: principles, applications and implementations," *Opt. Lasers Eng.* **45**, 304–317 (2007).
38. T. D. Creekmore and M. K. Eklund, "The possibility of skeletal anchorage," *J. Clin. Orthod.* **17**, 266–269 (1983).
39. Y-C. Tseng et al., "The application of mini-implants for orthodontic anchorage," *Inter. J. Oral Maxillofacial Surg.* **35**, 704–707 (2006).

40. S. Kuroda et al., "Clinical use of miniscrew implants as orthodontic anchorage: success rates and postoperative discomfort," *Am. J. Orthod. Dentofacial Orthop.* **131**, 9–15 (2007).
41. F. Chen et al., "Anchorage effects of a palatal osseointegrated implant with different fixation: a finite element study," *Angle Orthod.* **75**, 593–601 (2005).
42. P. R. Wedendal and H. I. Bjelkhagen, "Holographic interferometry on the elastic deformation of prosthodontic appliances as simulated by bar elements," *Acta Odontol. Scand.* **32**, 189–199 (1974).
43. H. Rydén, H. Bjelkhagen, and B. Mårtensson, "Tooth position measurements on dental casts using holographic images," *Am. J. Orthod.* **81**, 310–313 (1982).
44. J. A. Canut et al., "Effects of maxillary protraction determined by laser metrology," *Eur. J. Orthod.* **12**, 340–345 (1990).
45. H. Lang et al., "Determination of the dynamics of restored teeth by 3D electronic speckle pattern interferometry," *Lasers Surg. Med.* **34**, 300–309 (2004).
46. T. N. Campos et al., "Holographic interferometry method for assessment of static load stress distribution in dog mandible," *Braz. Dental J.* **17**, 279–284 (2006).
47. Y. Kojima and H. Fukui, "Effects of transpalatal arch on molar movement produced by mesial force: a finite element simulation," *Am. J. Orthod. Dentofacial Orthop.* **134**, 335.e1–335.e7 (2008).

Manoj Kumar received his MSc degree in physics from the University of Delhi in 2008, his MTech degree in instrumentation from National Institute of Technology Kurukshetra in 2011, and his PhD in optical engineering from Indian Institute of Technology Delhi, New Delhi in 2016. His research interest includes 3-D imaging, digital holography, speckle metrology, Talbot interferometry, and optical instrumentation. He is a member of SPIE and OSA.

Anshu Singh Birhman has completed her BDS from PDM Dental College and Research Institute, Bahadurgarh, Haryana, India, in 2014 and is pursuing her MDS from Department of Orthodontics and Dentofacial Orthopaedics, Manav Rachna Dental College Faridabad, Haryana, India. She specializes in Orthodontics and Dentofacial Orthopaedics.

Sridhar Kannan is a professor and head at Department of Orthodontics and Dentofacial Orthopaedics, Manav Rachna Dental College Faridabad, Haryana, India.

Chandra Shakher is an emeritus professor with the Instrument Design Development Centre at the Indian Institute of Technology Delhi, New Delhi. His research interest includes holography interferometry, speckle metrology, fiber-optic current sensors, optical coherence tomography, and laser-based instrumentation. He has more than 100 publications in international journals and 74 in conference proceedings. He is a fellow of the Indian National Academy of Engineering, senior member of OSA, and a fellow of SPIE.